Int. J. Electrochem. Sci., 12 **(2017)** 3030 – 3039, doi: 10.20964/2017.04.62

International Journal of
ELECTROCHEMICAL
SCIENCE
www.electrochemsci.org

Short Communication

The Electrochemical Behavior of Mg-Al-Zn-In-Ga Alloy as Anode Materials in Sodium Chloride Solution

Jiarun Li[1,2], *Kai Wan*[1,*] *and Ning Wang*[1,2]

[1] Key Laboratory of Marine Environmental Corrosion and Bio-fouling, Institute of Oceanology, Chinese Academy of Sciences, Qingdao 266071, Shandong, China;
[2] University of Chinese Academy of Sciences, Beijing 100049, China
[*]E-mail: wank711011@163.com

Received: 24 January 2017 / *Accepted:* 4 March 2017 / *Published:* 12 March 2017

The microstructures and electrochemical behavior of Mg-Al-Zn-In-Ga alloys are investigated by scanning electron microscopy (SEM), X-ray diffraction (XRD), galvanostatic oxidation, potentiodynamic polarization and electrochemical impedance spectroscopy (EIS). Their performances as anode for Mg-CuCl water-activated battery are also evaluated. It is found that appropriate Ga alloying (1 wt.%) could promote the electrochemical properties of Mg-Al-Zn-In alloy, but over alloying (2 wt.%) may increase the self-corrosion and decrease the discharge capability. The Mg-6%Al-3%Zn-1%In-1%Ga alloy with desirable corrosion resistance and discharge performance is a kind of promising anode materials for broadening the Mg power sources application.

Keywords: Magnesium alloy; Electrochemical behavior; Anode materials; Corrosion; Discharge

1. INTRODUCTION

Mg is a potential substitute for Al and Zn for serving as anode materials due to its desirable electrochemical properties, i.e., high negative standard potential of –2.34 V (vs. standard hydrogen electrode (SHE)), high theoretical specific discharge capacity of 2.2 A h g^{-1} and high theoretical energy density of 3.8 A h cm^{-1} [1-4]. Additionally, Mg has some other remarkable advantages, including easy acquisition in nature, low cost, safety for storing and environmentally acceptable properties, endowing Mg and its alloy a prospect of becoming widely used anode materials in chemical power source application [5, 6]. Nevertheless, there are several drawbacks of Mg for use as anode materials, such as voltage hysteresis, self-discharge, product adhesion and negative difference effect (NDE) in case of the anodic polarization, severely constrain the further development of Mg and its alloy in power sources field [7-10].

Doping with minor alloying elements is a recognized way in restraining the abovementioned defects and in optimizing the electrochemical properties of Mg alloys, including Al, Zn, Mn, Ca, In, Ga, etc. [11-16]. The influence of Al, Zn and Mn on the electrochemical properties of Mg-based sacrificial anode were investigated by Kim and Koo [11], they found that the increasing concentration of both three elements in Mg matrix can effectively alleviate the self-corrosion and improve the anode efficiency. Cao et al. [13] compared the discharge performances of Mg–Li–Al–Ce–Zn and Mg–Li–Al–Ce–Zn–Mn alloys. They found that Mn alloying improved anode utilization efficiency and power density by preventing the formation of dense oxide films and facilitating the removal of oxidation products. The Ca addition into Mg-Al-Mn alloy facilitating the generating of dense and thin discharge products was reported by Yuasa et al. [12]. They distributed the improved discharge activity to the less protective product film. Indium is an alloying element for activation of anode materials, the 1 wt.%~3 wt.% constituent of indium in aluminum could activate the alloy significantly in natural seawater [17]. Wang [14] and Jin [18] reported that the addition of indium in AP65 magnesium alloy promotes the electrochemical properties via decreasing the area ratio of cathode to anode. Ga is a traditional alloying element for Al activation [19], and some investigations had been carried out to broaden its application, such as Mg modification. Zhao et al. [15] found that the addition of Ga into Mg-Hg alloy could improve the discharge properties, attributing to the presence of $Mg_{21}Ga_5Hg_3$ phase, which diminished the charge-transfer resistance during the faradic reaction and adjusted the electronegativity discrepancy among different phases. Feng [16] found that adding Ga to the Mg matrix improved corrosion rate and discharge performance.

The corrosion and discharge behavior of Mg-Al-Zn-In alloys were investigated in our previous work [20], finding that the addition of 1 wt.%In to Mg-6 wt.%Al-3 wt.%Zn could obtain desirable anode performance due to the synergistic effect of grain refining, products self-peeling and dissolving-reprecipitation of In. Therefore, further improvement on the electrochemical performance of Mg-Al-Zn-In alloy is beneficial for the development of Mg as anode materials. In this work, a kind of new Mg-Al-Zn-In-Ga alloy was prepared by adding different amount of Ga (1 wt.% and 2 wt.%) into Mg-6 wt.%Al-3 wt.%Zn-1 wt.%In alloy, their corrosion and discharge behavior were investigated by material characterization and electrochemical tests. The performance of Mg-CuCl water-activated batteries was evaluated at different discharge current densities, aiming at obtaining a proper discharge condition and a kind of desirable Mg anode materials.

2. EXPERIMENTAL

2.1. Material preparation

The as-received AZ63 (Mg-6 wt.%Al-3 wt.%Zn) alloy (purchased from HongTai Magnesium Alloy Corporation, China), was melted in a furnace at 760 °C covered with sulfur powder to prevent from contacting with air. And then, the pre-weighted In (1 wt.%) and Ga (1 wt.% and 2 wt.%) ingots were added into the AZ63 melt, stirred for 5 min and held for 10 min. The mixed melt was poured into a preheated steel model (200 °C) with a dimension of ϕ 300 mm × 50 mm and cooled to ambient

temperature in air. The chemical compositions of the Mg-6%Al-3%Zn-1%In-1%Ga (donates as AZIG1) and Mg-6%Al-3%Zn-1%In-2%Ga (donates as AZIG2) alloys were analyzed by inductively coupled plasma mass spectrometry (ICP-MS), and the results are listed in Table 1.

Table 1. Chemical composition of AZIG1 and AZIG2 alloys (wt.%)

Alloys	Al	Zn	In	Ga	Fe	Cu	Ni	Mg
AZIG1	5.717	2.832	0.956	0.914	0.0008	0.0009	0.0005	Bal.
AZIG2	5.699	2.7806	0.943	1.896	0.0009	0.0009	0.0005	Bal.

Subsequently, the ingots were machined into different dimension coupons of 10 mm × 10 mm × 10 mm (for microstructure characterization and electrochemical tests) and 50 mm × 10 mm × 3 mm (for assembling battery), both of which were abraded to 5000 # using a SiC emery paper, successively. The prepared specimens were degreased with ethanol, dried by cold flow air, and stored in a desiccator.

2.2. Microstructure characterization

For microstructure observation, the pre-abraded 10 mm × 10 mm × 10 mm samples were polished by diamond grinding paste, cleaned with ethanol, wiped by 2.5 wt% nital solution and blow-dried by cool air. The microstructure of the two alloys were examined by scanning electron microscopy (SEM; Hitachi-S-3400N); Alloy phases were identified by X-ray diffraction (XRD; D/Max 2550, Rigaku) with Cu Kα radiation.

2.3. Electrochemical measurement

The electrochemical tests were conducted by a GAMRY 3000 electrochemical workstation in a three-electrode configuration (a platinum foil as counter electrode, a saturated calomel electrode as reference electrode and an Mg working electrode) containing 450 mL 3.5 wt.% NaCl solution. After 2 h immersion, electrochemical impedance spectroscopy (EIS) measurements with ±5 mV disturbing amplitude sinusoidal voltage were conducted within the frequency range of 100 kHz to 10 mHz at free corrosion potential (E_{corr}). Anodic and cathodic polarization tests were carried out at a scan rate of 0.167 mV s^{-1} from E_{corr} to ±500 mV after the EIS tests, respectively.

The galvanostatic current densities were designed at 5 mA cm^{-2} for 20 h and 10 mA cm^{-2} for 10 h, respectively, by considering the 100 mA h discharge electric quantity. Discharge capacity and utilization efficiency of anode were calculated using Eqs. (1) and (2), respectively:

$$\text{Discharge capacity (mAh g}^{-1}) = \frac{i \times A \times t}{M_a} \quad (1)$$

$$\text{Utilization efficiency: } \eta = \frac{M_t}{M_a} \times 100\% \quad (2)$$

where i is the current density (A cm^{-2}), A is the surface area (cm^2), t is the discharge period (h), and M_t and M_a are the theoretical and actual weight losses, respectively (g).

The anode performances of the AZIG1 and AZIG2 alloys for water-activated battery were evaluated using a battery testing system. A homemade CuCl electrode was adopted as the cathode. Both the exposed surfaces of the anode and cathode were 50 mm × 10 mm. The cell voltage was obtained by applying different current densities, (i.e. 5, 10, 20, 30, 40, 50, 75, 100, 125, 150, 175, and 200 mA cm^{-2}) over 5 min to achieve a stable voltage.

If not specified, all electrochemical measurements were replicated three to six times at ambient temperature depending on the reproducibility. All the electrolyte was prepared with demineralized water and all reagents used were of analytical purity grade.

3. RESULTS AND DISCUSSION

3.1. Microstructures

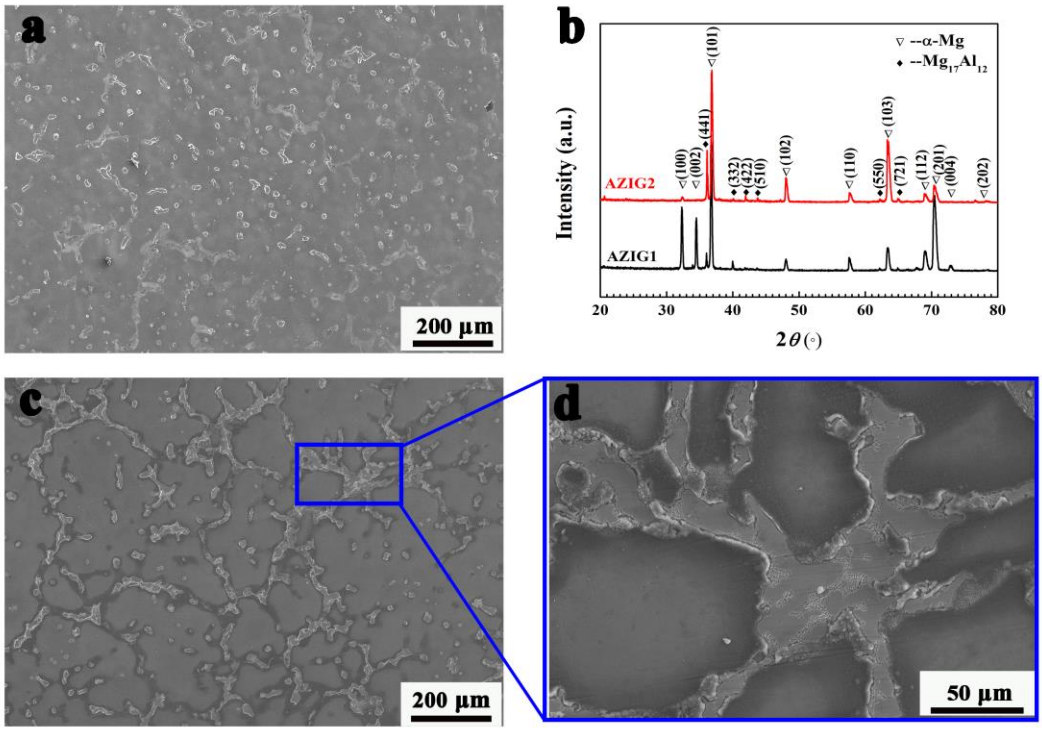

Figure 1. Microstructures of a) AZIG1, c) AZIG2 alloys and d) close-up view of c), b) XRD patterns of the two AZIG alloys.

The XRD patterns of AZIG1 and AZIG2 alloys are depicted in Fig. 1b. The major phase of the investigated alloys consists of α-Mg and β-$Mg_{17}Al_{12}$ phase, this is consistent with our previous work, which had added different amount of In into AZ63 alloy [20]. No In and Ga containing phase are detected probably due to their low concentration in Mg matrix, which are below the detection limit of XRD. The peak position of AZIG2 is slightly different from that of AZIG1, which may be attributed to

the lattice distortion induced by increasing amount of dissolved Ga in α-Mg [8]. Notably, the peaks intensity of AZIG2 representing β-$Mg_{17}Al_{12}$ phase is higher than that of AZIG1, indicating a promoted segregation effect aroused by increasing Ga concentration.

As shown in Figs. 1a, the microstructure of AZIG1 alloy comprises of α-Mg and discontinuous second phase segregating randomly both in α-Mg and along the grain boundaries. Different from AZIG1, the second phase of AZIG2 performs continuous net structure, which mainly segregates along the grain boundaries, implying the increasing Ga alloying could promote the segregation of the second phase. Fig. 1d shows the details of second phase framed in Fig. 1c, revealing that the second phase are main of β-$Mg_{17}Al_{12}$. This result is different from the second phase of Mg-Al-Zn-In alloy [20], which comprised of β-$Mg_{17}Al_{12}$ and eutectic α phase, indicating a depression of eutectic α phase generation by Ga alloying. Additionally, the increase of Ga alloying promotes the β-$Mg_{17}Al_{12}$ segregation revealed by comparing Figs. 1a and 1c, this is consistent with the results revealed by XRD patterns in Fig. 1b.

3.2. Corrosion behavior

The Nyquist plots of AZIG1 and AZIG2 are depicted in Fig. 2a. The EIS spectra of the two alloys comprise of one capacitive loop at high frequency and one inductive loop at low frequency, respectively. The capacitive loop in the first quartile is attributed to the property of double electric layer on the interface of electrode/electrolyte [21, 22], which could be thus represented by a charge transfer resistance (R_t) and a dielectric capacitance (C) in parallel connection. Here, the constant phase angle element (CPE_{dl}) is adopted to substitute the capacitance (C), aiming at describing the deviation effect of the electric double layer induced capacitor [14]. The inductive loop at the fourth quartile is attributed to the chemical reaction between the absorbed Mg^+ with H_2O in micro-pores [23, 24], which could be represented by a resistance ($R_{L\ Mg+}$) and an inductance (L_{Mg+}) in series connection. Owing to the abovementioned two physical/chemical processes take place simultaneously on the interface of electrode/electrolyte, the two units (R_t and CPE_{dl} in parallel connection, $R_{L\ Mg+}$ and L_{Mg+} in series connection) should be connected in parallel [25]. Consequently, the equivalent circuit for fitting the Nyquist plots of AZIG1 and AZIG2 is obtained as shown in Fig. 2b, where the R_s depicts the solution resistance between the tips of Luggin Capillary and working electrode. The fitting curves according to the equivalent circuit are shown in Fig. 1a and the calculated parameters are listed in Table 2. The charge transfer resistance, which is believed to characterize the difficulty of corrosion, can be ranked as AZIG2 < AZIG1, implying a promoted corrosion by increasing Ga alloying, which would be aroused by the increasing amount of micro-galvanic couples formed between α-Mg and β-$Mg_{17}Al_{12}$ phase.

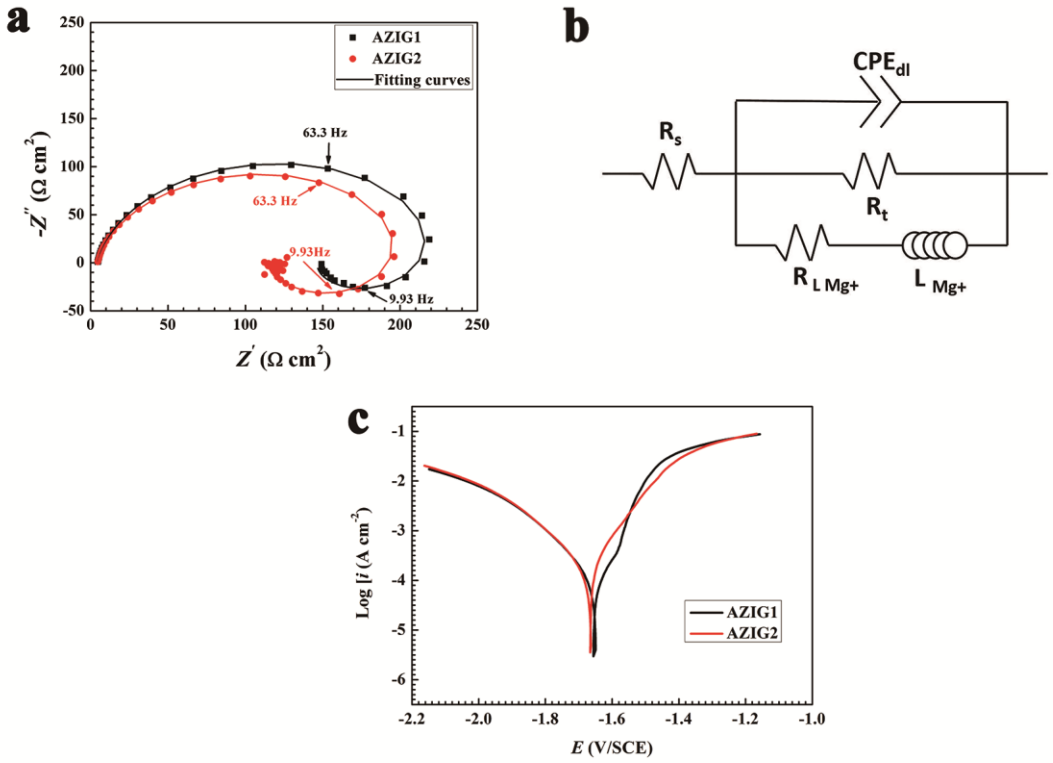

Figure 2. a) Nyquist diagrams, b) equivalent circuit for fitting and c) polarization curves of AZIG1 and AZIG2 alloys tested after 2 h immersion in 3.5 wt.% NaCl at ambient temperature.

Table 2. Tested electrochemical parameters after 2 h of immersion in 3.5 wt.% NaCl, calculated by fitting the electrochemical impedance spectra for AZIG1 and AZIG2 alloys.

Mg alloy	R_s (Ω cm_2)	R_t (Ω cm^2)	Y_{dl} (Ω^{-1} cm^{-2} s^n)	n_{dl}	R_{LMg+} (Ω cm^2)	L_{Mg+} (Ω cm^2 s)
AZIG1	4.52	243.8	1.52×10^{-5}	9.062×10^{-1}	338.7	57.84
AZIG2	4.53	222	1.68×10^{-4}	8.971×10^{-1}	234.9	3.99

The potentiodynamic polarizations from free corrosion potential (E_{corr}) to ±500 mV after 2 h immersion were carried out respectively and the curves are depicted in Fig. 2c. The corresponding corrosion parameters derived from the polarization curves are listed in Table 3. It is obvious that the cathodic reaction of hydrogen evolution dominates the corrosion of AZIG1 and AZIG2 by comparing the curve slopes in Fig. 2c [26, 27]. The cathodic branches of AZIG1 and AZIG2 are quite similar, indicating the increase of Ga alloying has little influence on cathodic reaction of Mg corrosion. The anodic polarization curve of AZIG2 performs smooth variation with increasing anodic potentials, owing to the surface of AZIG2 always be in the active dissolution state over the anodic polarization. Nevertheless, the anodic polarization curve of AZIG1 exhibits a passive region, which is probably

attributed to the broken down of the oxide film on alloy surface. The corrosion current densities obtained by Tafel extrapolation in Table 3 demonstrate that the AZIG1 is more corrosion resistive than AZIG2, this result also proves that the oxide film on AZIG1 is more protective than that of on AZIG2. Besides, the free corrosion potential of AZIG2 is more negative than that of AZIG1, implying an increased corrosion tendency by Ga alloying [9].

Table 3. Corrosion parameters of AZ63 and AZI alloys derived from the polarization curves.

Mg alloys	E_{corr}(vs. SCE)/V	i_{corr}/(μA cm^{-2})	b_c/(mV dec^{-1})
AZIG1	–1.649	132.4	–166.9
AZIG2	–1.663	161.2	–166.2

3.3. Discharge performance

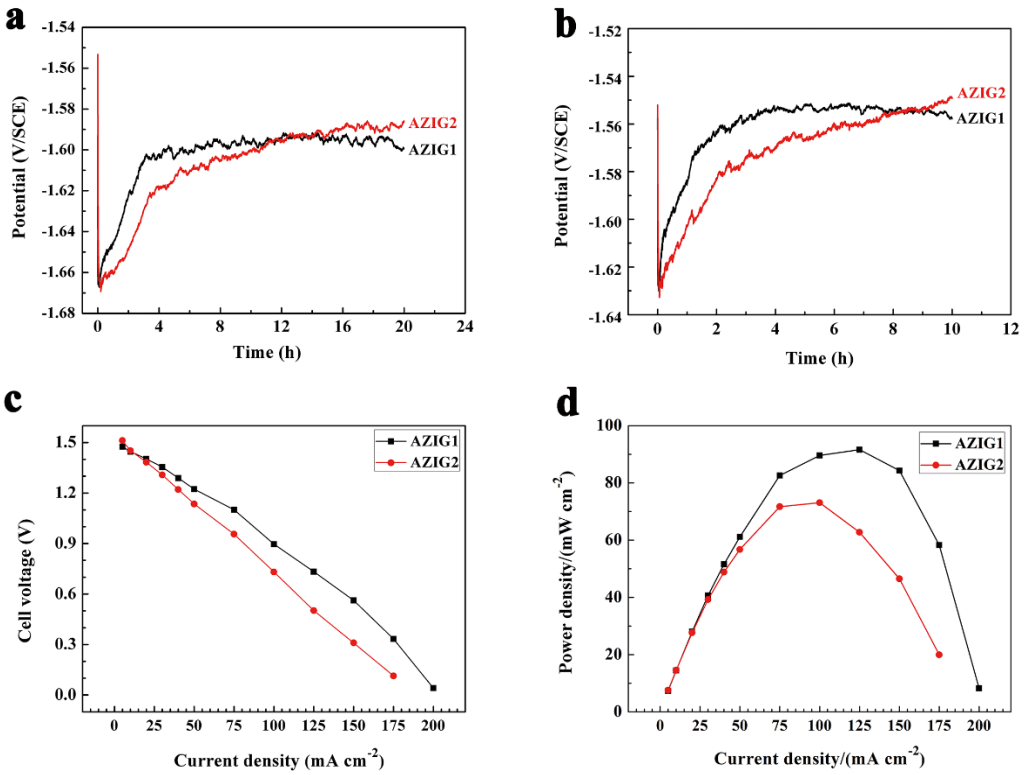

Figure 3. a) and b), potential–time curves of the AZIG1 and AZIG2 alloys at constant anodic current densities of 5 mA cm^{-2} and 10 mA cm^{-2}, respectively; Performance of Mg–CuCl water-activated batteries with the AZIG1 and AZIG2 anodes: c) plots of current density vs. cell voltage and d) plots of current density vs. power density in 3.5 wt.% NaCl at ambient temperature.

The potential-time curves of AZIG1 and AZIG2 at constant anodic current densities of 5 mA cm^{-2} for 20 h and 10 mA cm^{-2} for 10 h are shown in Figs. 3a and 3b, respectively. The curves of the

AZIG1 alloys perform similarly at different current densities, that is, increase at the outset of discharge and maintain at a certain potential range. Nevertheless, the potential curves of AZIG2 keep increasing until the end of test. The increasing potential with discharge time could be attributed to the generation and accumulation of products on electrode surface [20], and the consequent stable potential value is believed as an established dynamic equilibrium between the desorption and generation of discharge products [28]. Thus, it can be derived that the discharge products on AZIG1 has superior self-peeling ability than that of on AZIG2. The persistent potential increase of AZIG2 may lead to serious voltage hysteresis when it is adopted as anode for a battery and we can conclude that the AZIG1 is more suitable for serving as anode materials. The discharge parameters of the two alloys are listed in Table 4.

Table 4. Average discharge potential, discharge capacity, and utilizaiton efficiency of the AZIG1 and AZIG2 alloys at 5 mA cm^{-2} for 20 h and 10 mA cm^{-2} for 10 h, respectively in 3.5 wt.% NaCl.

Alloy	Condition	Average discharge potential (V vs.SCE)	Discharge capacity (mAh g^{-1})	Utilization efficiency (%)
AZIG1	5 mA cm^{-2}, 20 h	−1.607 ± 0.015	1403.56	63.89
	10 mA cm^{-2}, 10 h	−1.561 ± 0.015	1500.66	68.31
AZIG2	5 mA cm^{-2}, 20 h	−1.603 ± 0.021	1322.4	60.49
	10 mA cm^{-2}, 10 h	−1.571 ± 0.019	1561.35	71.42

The average discharge potentials of AZIG2 are kept varying with increasing immersion time due to the products accumulation on AZIG2 surface, which shifts its discharge potential towards positive orientation. Thus, the discharge potential of AZIG1 must be more negative than that of AZIG2 in the long term by comparing their discharge curves. As shown in Table 4, the standard deviations of AZIG1, which represent the fluctuation of the curves, are smaller than those of AZIG2, indicating a more stable discharge process of AZIG1, which implies a moderate product desorption process for AZIG1. Besides, the utilization efficiencies of AZIG1 at different discharge conditions are both higher than those of AZIG2, which further manifests that the AZIG1 is more suitable to serve as anode materials. Furthermore, the utilization efficiencies of the investigated alloys are higher than Mg-Al-Zn-In as reported in our previous work [20], validating a promoted electrochemical activity by Ga alloying.

The as-prepared AZIG1 and AZIG2 (50 mm × 10 mm × 3) specimens as anodes were assembled with a Cu/CuCl cathodes (50 mm × 10 mm × 3), using 3.5 wt.% NaCl as electrolyte. Their curves of voltage and power density vs. current density are depicted in Figs. 3c and 3d, respectively. Their cell voltages decay linearly with increasing current density, manifesting their strong anodic polarization and strong dependence on loop resistance [29]. By considering the curve slopes of the investigated anodes, the internal resistance of Mg-CuCl cell with AZIG1 anode is smaller than that of the cell with AZIG2 anode, which could be interpreted by its superior capability of anodic polarization, that is, the increase of polarization resistance for AZIG1 anode is less than that of AZIG2 anode throughout the process of increasing current density. As shown in Fig. 4d, the AZGI1 anode possesses

the largest peak power density of 91.63 mW cm^{-2} at 125 mA cm^{-2} current density, this result is higher than those of Mg-Li-Al-Ce-Zn and Mg-Li-Y anodes as reported in Refs [8, 29], and comparable with (Mg-Li-Al-Ce-Zn-Mn)-H_2O_2 semi-fuel cell [8]. Hence, AZGI1 alloy is a kind of suitable anode material for Mg power sources application.

The discharge morphologies of AZIG1 and AZIG2 after Mg-CuCl cell tests are depicted in Fig. 4. Notably, there is little discharge products sticking on the electrode surface, which may probably due to the anodic polarization at the end of cell test (approximate 200 mA cm^{-2}), arousing fierce hydrogen evolution. It is believed that the hydrogen evolution may induce stirring effect on electrode surface, facilitating the removal of products [25]. The dissolution of AZIG1, identified by tiny second phase, is obviously more uniform than that of AZIG2, which performs local dissolution characteristic as marked in Fig. 4b. The undissolved α-Mg grains on AZIG2 surface could not effectively participate in the anodic discharge due to the presence of continuously surrounding β-$Mg_{17}Al_{12}$ phase, which is proved to be insulator, and thus, decrease the discharge capacity.

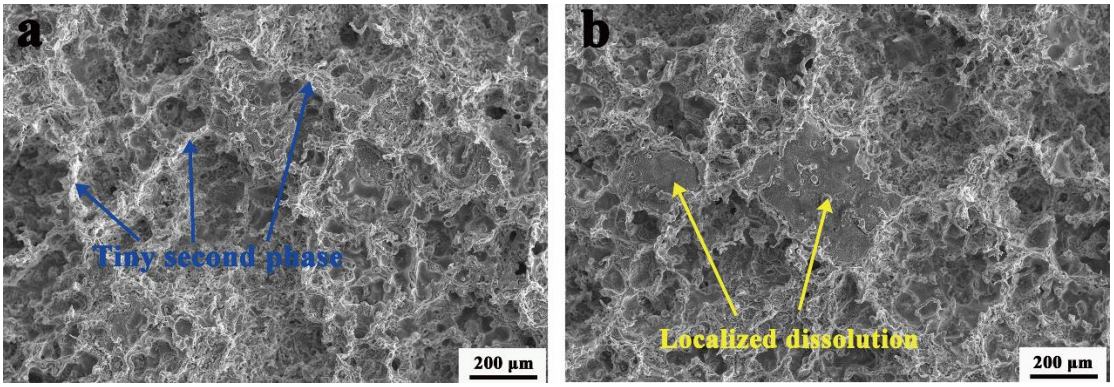

Figure 4. Morphologies of a) AZIG1 and b) AZIG2 anodes after discharge test of Mg-CuCl cell in 3.5 wt.% NaCl at ambient temperature.

4. CONCLUSIONS

A kind of new Mg-Al-Zn-In-Ga alloys were prepared and their corrosion and discharge performance have been investigated in this paper, and several conclusions are drawn as follows:

(1) The increase of Ga alloying promotes the segregation of β-$Mg_{17}Al_{12}$ phase and depresses the generation of eutectic α phase. Besides, the increasing Ga concentration has little influence on grain size.

(2) The corrosion rate of AZIG1 is smaller than that of AZIG2, which is probably owing to the high amount of β-$Mg_{17}Al_{12}$ phase in AZIG2 alloy by forming more micro-cells with α-Mg grains. Additionally, it can be deduced that the oxide film on AZIG1 is more protective by considering the passive region of anodic polarization curve.

(3) The Mg-6%Al-3%Zn-1%In-1%Ga alloy, with the properties of high corrosion resistance, high discharge capacity, high power density and uniform dissolution morphology, is a promising candidate for serving as anode materials in Mg primary power sources field.

ACKNOWLEDGEMENTS
The authors wish to acknowledge the financial support of the China Postdoctoral Science Foundation (No. 2016M602198)

References

1. J. Besenhard, M. Winter, *Chemphyschem*, 3 (2002) 155-159.
2. Z. Yu, G. Shi, D. Ju, *Int. J. Electrochem. Sci.*, 9 (2014) 6668-6676.
3. M. Shinohara, E. Araki, M. Mochizuki, T. Kanazawa, K. Suyehiro, *J. Power Sources*, 187 (2009) 253-260.
4. S. Johnston, Z. Shi, A. Atrens, *Corros. Sci.*, 101 (2015) 182-192.
5. M. Yuasa, X. Huang, K. Suzuki, M. Mabuchi, Y. Chino, *J. Power Sources*, 297 (2015) 449-456.
6. H. Zhao, P. Bian, D. Ju, *J. Environ. Sci-China*, Supplement 1 (2009) S88-S91.
7. T. Zhang, Z. Tao, J. Chen, *Mater. Horiz.*, 1 (2014) 196-206.
8. D. Cao, L. Wu, G. Wang, Y. Lv, *J. Power Sources*, 183 (2008) 799-804.
9. D. Cao, L. Wu, Y. Sun, G. Wang, Y. Lv, *J. Power Sources*, 177 (2008) 624-630.
10. F. Sapountzi, J. Gracia, C. Weststrate, H. Fredriksson, J. Niemantsverdriet, *Prog. Energy Combust. Sci.*, 58 (2017) 1-35.
11. J. Kim, S. Koo, *Corrosion-US*, 56 (2000) 380-388.
12. M. Yuasa, X. Huang, K. Suzuki, M. Mabuchi, Y. Chino, *J. Power Sources*, 297 (2015) 449-456.
13. D. Cao, L. Wu, G. Wang, Y. Lv, *J. Power Sources*, 183 (2008) 799-804.
14. N. Wang, R. Wang, C. Peng, B. Peng, Y. Feng, C. Hu, *Electrochim. Acta*, 149 (2014) 193-205.
15. J. Zhao, K. Yu, Y. Hu, S. Li, X. Tan, F. Chen, Z. Yu, *Electrochim. Acta*, 56 (2011) 8224-8231.
16. Y. Feng, R. Wang, C. Peng, *Corrosion-US*, 67 (2011) 055003-055001-055003-055006.
17. A. Zazoua, N. Azzouz, *Mater. Design*, 29 (2008) 806-810.
18. H. Jin, R. Wang, C. Peng, K. Shi, Y. Feng, *J. Cent. South. Univ.*, 19 (2012) 2086-2093.
19. S. Toriyama, T. Mae, K. Arai, *Mater. Trans.*, 39 (1998) 404-412.
20. J. Li, K. Wan, Q. Jiang, H. Sun, Y. Li, B. Hou, L. Zhu, M. Liu, *Metals-Basel*, 6 (2016).
21. F. Zucchi, V. Grassi, A. Frignani, C. Monticelli, G. Trabanelli, *J. Appl. Electrochem.*, 36 (2006) 195-204.
22. R. Udhayan, D. Bhatt, *J. Power Sources*, 63 (1996) 103-107.
23. T. Zhang, Y. Shao, G. Meng, Z. Cui, F. Wang, *Corros. Sci.*, 53 (2011) 1960-1968.
24. J. Chen, J. Wang, E. Han, J. Dong, W. Ke, *Electrochim. Acta*, 52 (2007) 3299-3309.
25. J. Li, Q. Jiang, H. Sun, Y. Li, *Corros. Sci.*, 111 (2016) 288-301.
26. G. Song, A. Atrens, *Adv. Eng. Mater.*, (1999) 11-33.
27. G. Makar, J. Kruger, *Int. Mater. Rev.*, 38 (1993) 138-153.
28. A. Suresh Kannan, S. Muralidharan, K. Sarangapani, V. Balaramachandran, V. Kapali, *J. Power Sources*, 57 (1995) 93-98.
29. Y. Lv, M. Liu, Y. Xu, D. Cao, J. Feng, R. Wu, M. Zhang, *J. Power Sources*, 239 (2013) 265-268.